

Iodine Frequency Reference on a Sounding Rocket

Klaus Döringshoff,^{1,*} Franz B. Gutsch,¹ Vladimir Schkolnik,¹ Christian Kürbis,² Markus Oswald,³ Benjamin Pröbster,^{3,4} Evgeny V. Kovalchuk,¹ Ahmad Bawamia,² Robert Smol,² Thilo Schuldt,^{3,5} Matthias Lezius,⁴ Ronald Holzwarth,⁴ Andreas Wicht,² Claus Braxmaier,^{3,5} Markus Krutzik,^{1,2} and Achim Peters^{1,2}


¹*Humboldt-Universität zu Berlin, Institut für Physik, Berlin 12489, Germany*

²*Ferdinand-Braun-Institut, Leibniz-Institut für Höchstfrequenztechnik, Berlin 12489, Germany*

³*Universität Bremen, Zentrum für angewandte Raumfahrttechnologie und Mikrogravitation (ZARM), Bremen 28359, Germany*

⁴*Menlo Systems GmbH, Martinsried 82152, Germany*

⁵*Deutsches Zentrum für Luft- und Raumfahrt (DLR), Institut für Raumfahrtssysteme, Bremen 28359, Germany*

 (Received 18 December 2018; revised manuscript received 22 March 2019; published 24 May 2019)

We build a self-contained optical absolute frequency reference at 1064 nm based on the rovibronic transition R(56)32-0 in molecular iodine and operate this instrument in space on a sounding rocket mission. The frequency reference uses a microintegrated extended cavity diode laser and a quasimonolithic spectroscopy module for modulation transfer spectroscopy, providing frequency instability of 2×10^{-13} for averaging times of 100 s. To demonstrate the autonomous operation of our reference, we perform an absolute frequency measurement using a chip-scale atomic clock and an optical frequency comb during a 6-min-long space flight.

DOI: [10.1103/PhysRevApplied.11.054068](https://doi.org/10.1103/PhysRevApplied.11.054068)

I. INTRODUCTION

Frequency-stable laser systems are a key technology in precision experiments and have recently become applicable in space. Optical frequency references based on cavities, atoms, or molecules allow for precise laser frequency stabilization and thus enable, for example, high-precision laser ranging in space missions. Examples are the gravity recovery and climate experiment-follow-on (GRACE-FO) mission [1,2] that was recently put in operation, the planned laser interferometer gravitational wave observatory LISA [3], and future global satellite navigation systems based on optical clocks [4,5]. In the context of these and other missions, frequency references based on optical cavities [6,7] and unequal-arm-length interferometers [8,9] have been developed as compact, ruggedized instruments for application in space, featuring good short-term instability.

One way to also realize low long-term instability is the stabilization to atomic or molecular transitions, providing an advantage in accuracy over relative frequency references. Together with optical frequency combs, such absolute references can further be operated as optical clocks with instability relevant for global navigation satellite systems (GNSS). Several such systems are under

investigation today at various wavelengths, based on thermal calcium beams [10–12] or hot vapor cells using single- [13] or two-photon transitions in rubidium [14,15].

Another, already matured frequency reference is based on saturation spectroscopy of molecular iodine using the second harmonic of the narrow linewidth Nd:yttrium-aluminum-garnet (YAG) laser at 1064 nm. These systems rely on the modulation-transfer spectroscopy (MTS) technique applied to the rovibronic transition R(56)32-0, featuring narrow transitions with a natural linewidth of 300 kHz [16]. The hyperfine spectrum of this transition was studied in detail [17], the absolute frequency was accurately measured with an uncertainty of 1.1 kHz by Nevsky *et al.* [18], and Ye *et al.* demonstrated operation of a molecular iodine optical clock over the course of a full year [19]. In the past decade, several groups realized compact and portable iodine references with fractional frequency instability in the low 10^{-15} regime [20,21] and subjected their setups to environmental tests [22]. We believe that, using available technology at 1064 nm, developed in the context of the LISA and the GRACE-FO mission and established in satellite laser communication terminals, such systems can be developed for spaceborne instruments on relatively short time scales.

Here, we present a stand-alone iodine frequency reference at 1064 nm, named JOKARUS, that is based on a microintegrated extended-cavity diode laser (ECDL)

*klaus.doeringshoff@physik.hu-berlin.de

[23,24] in a master oscillator plus power amplifier (MOPA) configuration. JOKARUS was built to demonstrate the maturity of our technology and its applicability in space missions. To this end, we operate JOKARUS on a sounding rocket mission and thereby prove the autonomous operation of an optical iodine frequency reference. We compare the optical frequency to a chip-scale atomic clock (CSAC) via a self-referenced frequency comb on the ground and in space.

This paper is organized as follows. Section II describes the optical iodine frequency reference and its autonomous operation, as well as the optical frequency comb used to verify the frequency instability of the iodine reference aboard the sounding rocket. Section III presents results on the characterization of the frequency instability of the iodine frequency reference obtained on the ground and from the operation in space. Finally, in Sec. IV, we summarize the results and give a conclusion.

II. EXPERIMENTAL SETUP

A. Iodine frequency reference JOKARUS

The iodine frequency reference JOKARUS is based on modulation transfer spectroscopy of the rovibronic transition $R(56)32-0 a_1$ in molecular iodine using a microintegrated ECDL in a MOPA configuration. The modular payload is made up of four aluminum trays mounted on a water-cooled heat sink and an electronics stack on top. A photograph and a schematic of the JOKARUS payload are shown in Figs. 1 and 2, respectively. Here, we give a brief overview of the system and highlight changes to the initial design described in Ref. [25].

1. Optics

The ECDL MOPA laser source provides a fiber-coupled optical power of up to 550 mW at 1064 nm with a linewidth of 25 kHz ($10 \mu\text{s}$) (according to the β -separation line method [26]). The free spectral range (FSR) of the extended cavity is 4.8 GHz and the coarse tuning range of the ECDL is 53 GHz. The ECDL features a mode-hop-free tuning range of 8 GHz when using the injection current only [24], which covers three transitions in iodine, namely $R(56)32-0$ and the overlapping transitions $P(53)32-0$ and $P(103)34-0$.

The laser is followed by an optical isolator and a fiber splitter that separates 3 mW of optical power for beat-note measurements; see Fig. 2(d). The major part of the light is used for MTS and therefore split into pump and probe beams. The latter is directly connected to a mating sleeve at the housing of the laser system tray; see Fig. 1(e). The pump beam is frequency-shifted by 150 MHz using an acousto-optic modulator (AOM, T-M150-0.4C2G-3-F2P, Gooch & Housego) and phase-modulated by 300 kHz with

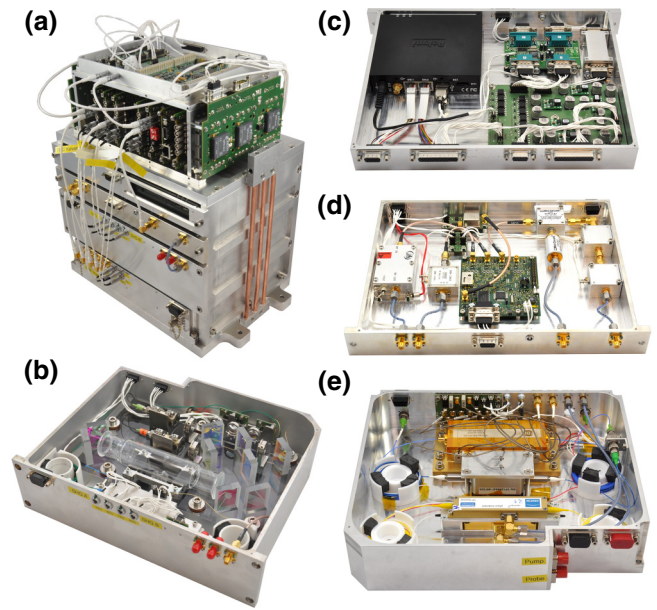


FIG. 1. Photographs of the JOKARUS payload. (a) JOKARUS payload. The payload has dimensions of $340 \times 255 \times 355 \text{ mm}^3$ ($w \times d \times h$), corresponding to a volume of 31 l, and has a total mass of 22.6 kg. (b) Spectroscopy tray including the spectroscopy module and the SHG modules. (c) Control computer tray including control computer, dc/dc converter, and RS232 interface. (d) rf tray including DDS, rf amplifier for the AOM, the EOM and the MTS signal, mixer and lowpass filter. (e) Laser system including the ECDL MOPA, an optical isolator, as well as the AOM and the EOM.

a modulation index of about 1 by an electro-optic modulator (EOM, PM1064, Jenoptik) whose output fiber is then also connected to a mating sleeve on the laser system tray.

The pump and probe beams are then fiber-coupled to the spectroscopy tray with optical powers of 25 and 47 mW, respectively [Fig. 2(b)], which includes two periodically poled lithium niobate (PPLN) waveguide second-harmonic generation (SHG) modules (WH-0532-000-F-B-C, NTT Electronics). These modules frequency-double the light to 532 nm, providing 4.2 and 1.4 mW for the pump and probe beam path, respectively. Their output fibers are connected to a quasimonolithic spectroscopy module; see Fig. 1(b). The spectroscopy module comprises a MTS setup on a $246 \times 145 \times 27 \text{ mm}^3$ fused silica bench and has a total mass of 2.7 kg. The setup features a 15-cm-long iodine absorption cell filled with ultrapure $^{127}\text{I}_2$ at an unsaturated pressure of about 1.3 Pa, corresponding to a cold finger temperature of -10°C . Using an unsaturated cell allows us to omit the usual cooling and temperature control of a cold finger and was previously tested in another setup showing frequency noise below $40 \text{ Hz/Hz}^{-1/2}$ for Fourier frequencies between 10 mHz and 10 Hz [22], which is compatible with the requirement on white laser frequency noise of the LISA and the GRACE-FO mission of $280 \text{ Hz/Hz}^{-1/2}$

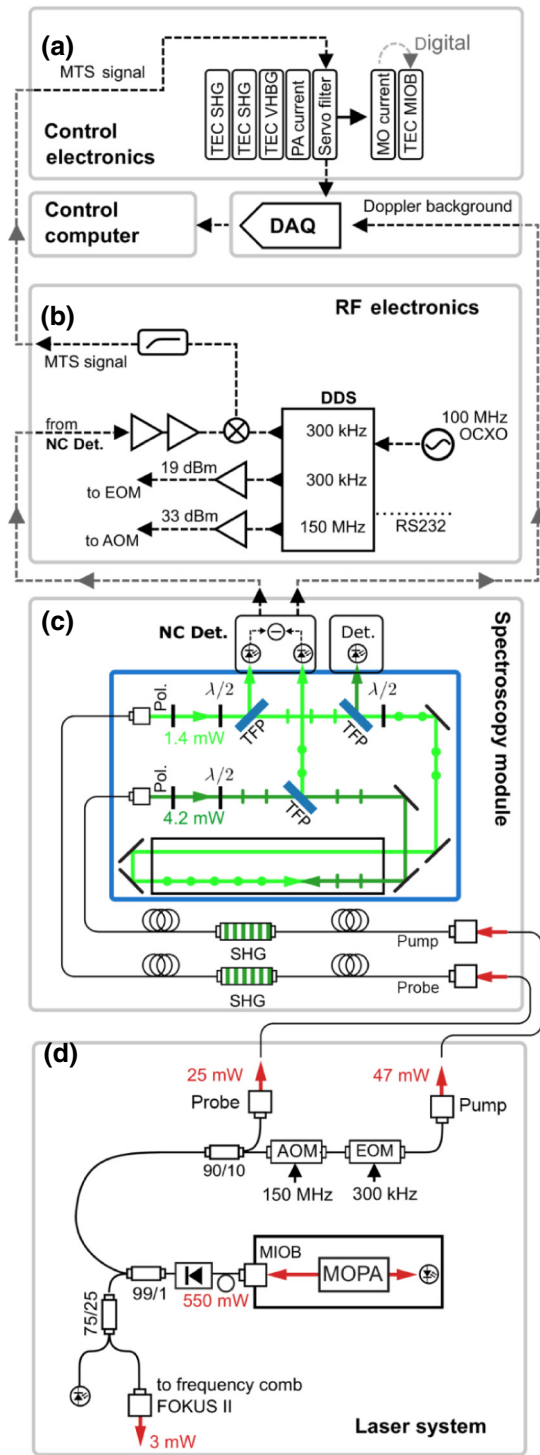


FIG. 2. Schematic of JOKARUS. (a) Control electronics, data acquisition unit for spectroscopy signals and system monitoring, and control computer. (b) rf system. (c) Modulation transfer spectroscopy module with balanced detection. (d) Laser system with noise-canceling detector (NC Det.), thin film polarizer (TFP), polarizer (Pol.), data acquisition unit (DAQ), microintegrated optical bench (MIOB), thermoelectric cooler (TEC), second harmonic generation module (SHG), volume holographic Bragg grating (VHBG) of the ECDL, master oscillator (MO), power amplifier (PA).

and $40 \text{ Hz/Hz}^{-1/2}$, respectively. The absorption cell is double-passed by the pump and probe beams with crossed polarization [see Fig. 2(b)], with beam diameters of 2 mm, corresponding to a time-of-flight broadening below 13 kHz and pump beam intensity of 1.4 mW mm^{-2} . We implement balanced detection of the spectroscopy signal using a reference beam (1.2 mW) that bypasses the iodine cell, the actual probe beam (0.2 mW), and a noise-canceling detector [27]; see Fig. 2(b). This configuration is useful when using a Nd:YAG nonplanar ring oscillator (NPRO) laser, as it efficiently suppresses the intensity noise of the NPRO laser in the MTS signal [21,22]. However, it turns out to be ineffective when used with the ECDL, as discussed in Sec. III. This result is presumably due to the conversion of laser frequency noise to intensity noise on the probe beam in the iodine cell, which is not present on the reference beam and therefore not canceled.

2. Electronics

The necessary rf signals are generated and processed in the rf tray depicted in Fig. 1(d). The frequencies for the AOM and the EOM are derived from a DDS generator (DDS9m, Novatech Instruments) that is referenced to a 100-MHz oven-controlled crystal oscillator (OCXO); see Fig. 2(c). Two rf amplifiers drive the AOM and EOM with 32 and 19 dBm, respectively. The MTS signal is received from the spectroscopy module, amplified and demodulated using an analog double-balanced mixer, lowpass-filtered, and fed to the control electronics stack as well as a data acquisition unit (DAQ); see Fig. 2(a).

Control electronics for the iodine reference is consolidated in an electronics stack provided by Menlo Systems; see Fig. 1(a). It comprises an embedded system and several control cards. Two temperature controllers are used for the temperature of the housing of the ECDL (25.5°C) and the volume-holographic Bragg grating of the ECDL (27°C). Two additional temperature controllers maintain the phase-matching condition for the SHG modules with temperatures of 47°C and 40°C , respectively. Two current drivers are used to drive the master oscillator diode chip and the ridge waveguide power amplifier at 120 and 1200 mA, respectively, and an analog feedback control servo filter is used for frequency-stabilizing the ECDL.

A computer program running on a compact fanless computer (exone FANLESS Pokini Z530) system is used to control the embedded system. It commands a controlled start-up and shutdown sequence for the laser system and self-controlled operation, including autonomous locking of the laser frequency to the selected component a_1 of the rovibronic transition R(56)32-0, detailed in Sec. II A 4.

3. System budgets

JOKARUS has a mass of 22.6 kg and dimensions of $340 \times 255 \times 355 \text{ mm}^3$ ($w \times d \times h$), corresponding to a

volume of 31 l. Aboard the sounding rocket, JOKARUS is housed in a cylindrical dome with a diameter of 375 mm and height of 420 mm and is pressurized at 115 kPa. The whole system is powered with 24 V from a battery and a dc/dc converter provided by the service system of the sounding rocket and consumes less than 100 W.

Because of the power dissipation and the resulting heat buildup of the system in the dome, we had to change JOKARUS from the original design [25]; we integrated fans below the electronics stack and added heat pipes to conduct the heat from the electronics down to the water-cooled heat sink; see Fig. 1(a).

For qualification of JOKARUS with regard to the sounding rocket flight, we shake the idle system with rms accelerations of 8.8g in a frequency band between 20 Hz and 2 kHz for 60 s in each axis.

4. Experiment control

For autonomous operation of JOKARUS aboard the sounding rocket, we developed a software written in Python that runs on the control computer. We made the experiment control software's full source code publicly available under a permissive license [28]. During flight, the control computer commands the embedded systems of the control electronics based on timer and hardware commands issued by the sounding rocket's service module.

The main feature of the software is an autolock algorithm that reads spectroscopy signals from the DAQ and controls laser parameters via the embedded system to lock the laser frequency to the selected transition in the approximately 8-GHz tuning range of the laser. To this end, the software scans the laser frequency via the injection current and identifies the Doppler background of the transition from the logarithmic output of the noise-canceling detector [27]. The Doppler broadened lines of the transition R(56)32-0 and the overlapping transitions P(53)32-0 and P(103)34-0 are simply distinguished by their respective amplitudes. First, the algorithm centers the laser frequency on the Doppler background of the chosen transition R(56)32-0, then jumps into the capture range of the preselected hyperfine structure component, and finally engages the lock. A single scan takes 0.5 s plus 1.5 s for data transfer and the fit of the Doppler broadened signal. Several scans (typically less than 10) are used to verify a sufficiently low drift rate of the laser before the actual lock is engaged. To ensure a reliable lock acquisition, the integrator of the control loop servo filter is biased such that it rails the laser frequency toward red when the lock is enabled *off*-resonance. This way, the general capture range equals the one-sided dynamic range of the control signal (approximately 0.7 GHz) instead of being limited to the linewidth of the Doppler-free MTS signal (approximately 1 MHz) and the lock can reliably be engaged when the laser frequency is blue detuned from the targeted transition. For the

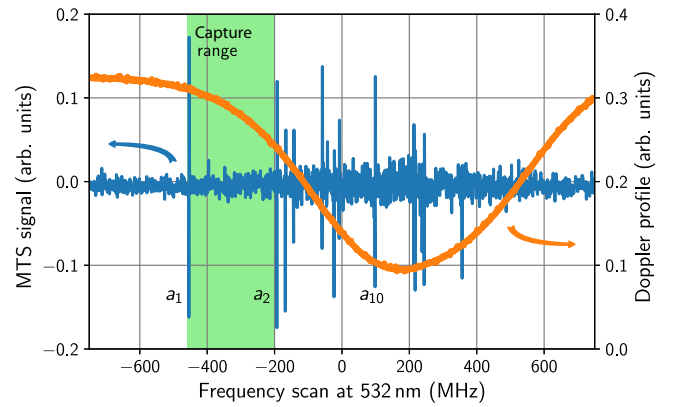


FIG. 3. Spectra of transition R(56)32-0 taken by the autonomy algorithm in space prior to locking to component a_1 . The x axis is calculated from the ramp applied to the injection current and the tuning coefficient of the laser. The MTS spectrum is low-pass filtered with a corner frequency of 40 kHz recorded with 2560 samples with 16-bit resolution in 500 ms, resulting in a spectral resolution of only 0.9 MHz; thus, some spectral components appear clipped. The Doppler profile is recorded from the logarithmic output of the noise-canceling detector [27] and used for the autonomous lock acquisition. The capture range of the lock between a_1 and a_2 is indicated in green.

component a_1 , the capture range equals the range between the lines a_1 and a_2 , i.e., 130 MHz at 1064 nm; see Fig. 3. Frequency stabilization is realized with fast feedback control via the MO injection current with a bandwidth of 10 kHz with proportional gain and two integrators at corner frequencies of 520 and 137 Hz. Slow feedback is implemented via software, adjusting the injection current set point once per second to keep the fast feedback control signal centered in its dynamic range. Additionally, the temperature of the ECDL's housing is adjusted every 90 s to compensate for temperature drifts, thus keeping the injection current in a safe range, while the grating of the ECDL is kept at a constant temperature.

B. Dual frequency comb

In order to measure the absolute optical frequency of JOKARUS, its output is connected via fiber to the independent FOKUS II payload. FOKUS II is the second-generation optical frequency comb device developed for sounding rocket experiments by Menlo Systems; see Fig. 4. Compared to the first demonstrator FOKUS I [29], the system was built up from scratch in order to further optimize the mass, volume, and power consumption.

Newly developed optics as well as digital and analog electronics allow us to accommodate two independent frequency combs (combs A and B) and beat-detection-units (BDUs) within a budget of 10 kg, 7 l, and 66 W, thus reducing these parameters by a factor of 2 compared to FOKUS I. Moreover, the system is designed for

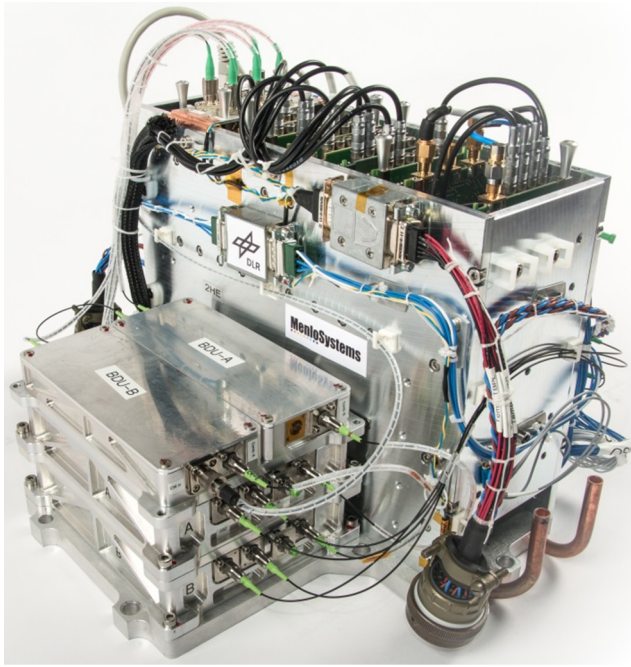


FIG. 4. Photograph of the FOKUS II system. The entire optics with two BDUs and two frequency combs are shown on the front left. The back part is used by the control and supply electronics. The payload has a volume of 7 l and the mass is 10 kg.

in-vacuum operation, requiring an overhauled thermomechanical design and advanced passive cooling for the high power diode drivers and the dc/dc converters. Each comb consists of a polarization-maintaining-fiber-based Figure-9 100-MHz oscillator operating at (1560 ± 25) nm (FWHM), an erbium-doped fiber amplifier (EDFA), and a periodically poled lithium niobate waveguide-based f - $2f$ interferometer.

The beat detection units combine the comb light with the JOKARUS light at 1064 nm, without any further amplification or second harmonics generation. The combs' two degrees of freedom, namely the repetition rate and the carrier-envelope-offset frequency, are actively controlled on a microintegrated free-space optical setup. In our attempt, the required components (collimator, beam splitters, end mirror, optical modulators) are soldered onto a gold-plated ceramics carrier, thus avoiding possible issues from outgassing adhesives or other volatile products in vacuum.

By utilizing a dual comb system (see Fig. 5), the mode numbers and consequently the absolute frequency of JOKARUS can be determined without additional means like an external wavemeter. With the two combs, referenced to a miniaturized low noise chip scale atomic clock (Microsemi LNCSAC) and locked at slightly different repetition rates, a continuous mode number determination is achieved [30].

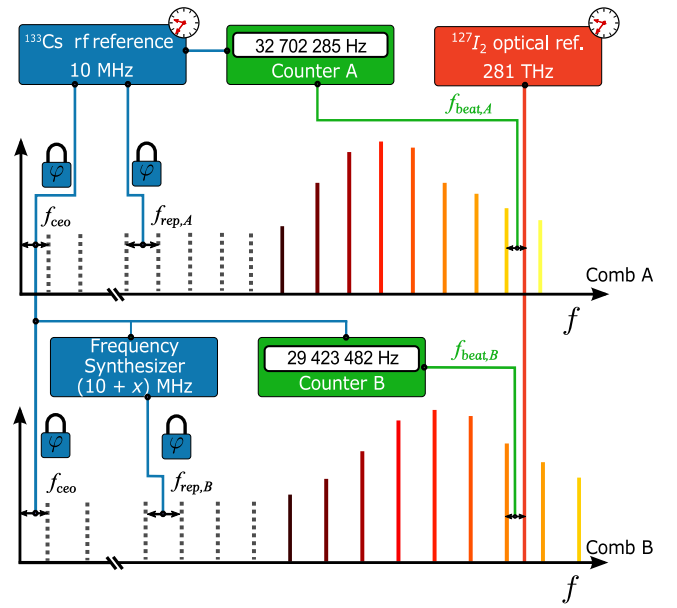


FIG. 5. Schematic of the dual comb measurement with JOKARUS. The repetition rate of comb A is locked to a miniaturized atomic clock, while comb B is tunable via a rf frequency synthesizer. In both combs, the carrier envelope offset is self-referenced and locked to the same cesium reference. Two different beat signals with the JOKARUS payload are generated and counted simultaneously, allowing an absolute optical frequency determination.

III. RESULTS

The following section presents the analysis of the frequency instability of the iodine frequency reference on the ground and the measurements taken during the sounding rocket mission.

A. Ground

To characterize the frequency instability of the iodine frequency reference JOKARUS, we perform beat-note measurements with a cavity-stabilized laser system as described previously [21,22] and a laboratory iodine reference. The cavity provides a previously verified frequency instability below 3×10^{-15} for averaging times between 0.1 and 10 s and a linear drift of the order of 10^{-16} s^{-1} .

From the time record of the beat notes, we calculate the Allan deviation displayed in Fig. 6. The Allan deviation shows a short-term instability of $1.5 \times 10^{-13} / \sqrt{\tau}$, where τ is the averaging time in seconds, between 10 ms and 0.3 s. Between 0.3 and 100 s, the Allan deviation shows a persistent bump. The origin of the increased frequency instability on these time scales is under investigation and seems to be related to air currents over the setup. For averaging times above 1000 s, the Allan deviation of the beat note with the cavity follows a trend of $3 \times 10^{-16} \times \tau$ that is mainly attributed to the isothermal creep of the reference ultra low expansion (ULE) cavity, while the beat note

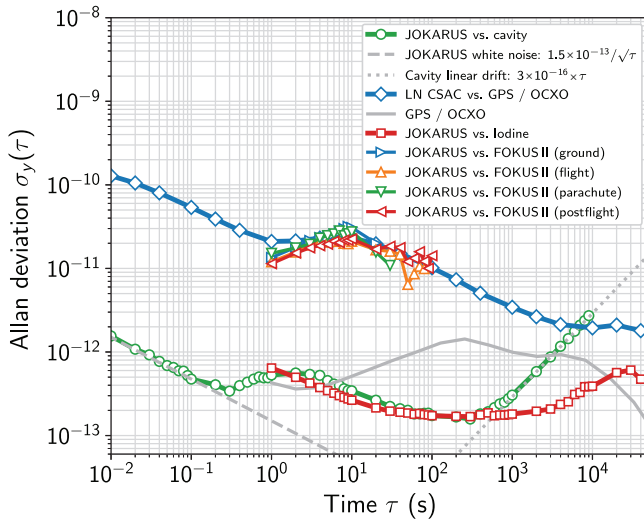


FIG. 6. Allan deviation of the beat note between the iodine frequency reference JOKARUS and a cavity-stabilized laser (\circ) and another iodine frequency reference (\square). The frequency instability of the LNCSAC is measured in comparison to a GPS disciplined OCXO and is shown for comparison (\diamond). The instability of the beat note between JOKARUS and FOKUS II for the different phases of the mission [ground (\triangleright), flight (\triangle), parachute (∇), postflight (\triangleleft)] match the instability of the LNCSAC.

with the iodine reference shows a flicker noise floor of 2×10^{-13} between 20 and 2000 s of averaging time.

The frequency instability for averaging times below 0.3 s is limited by the detection noise of the MTS signal that is deteriorated by the phase modulation (PM)/amplitude modulation (AM) conversion of laser frequency noise in the absorption cell [31,32], not suppressed by the balanced detection scheme. This effect was not sufficiently considered in the design of the system, but might be mitigated by passing the reference beam also through the absorption cell, as demonstrated for Cs spectroscopy by Hori *et al.* [33].

With respect to the sounding rocket mission, the instability of the JOKARUS iodine frequency reference does not limit the precision of the frequency measurements given the instability of 2×10^{-11} of the rf reference (LNCSAC, Microsemi) used in the self-referenced frequency comb; see Fig. 6 (\diamond).

B. Space flight

In the following, we describe the sounding rocket flight, the operation of JOKARUS, the data acquisition, and finally the analysis of the data.

JOKARUS was launched aboard the TEXUS 54 sounding rocket at 10:30 a.m. on May 13, 2018, from the Esrange Swedish Space Center (SSC), together with FOKUS II. The flight profile and the different phases of the flight are indicated in Fig. 7, together with accelerations and the beat note between JOKARUS and the frequency comb A of

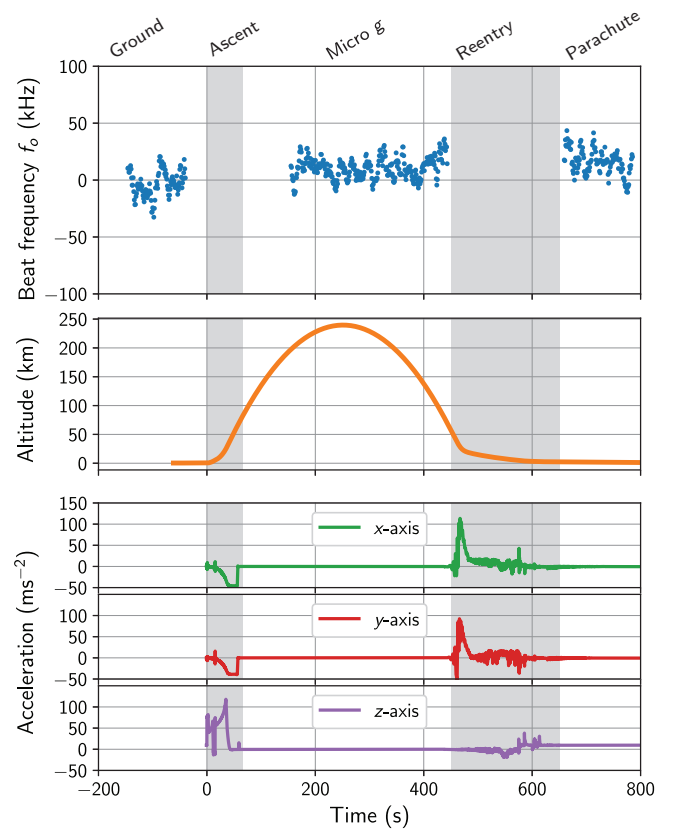


FIG. 7. Time records of the flight. Top: Beat-note frequency between the JOKARUS and the frequency comb FOKUS II at 1064 nm ($f_0 = 30.9855$ MHz). The lengths of the time records are 107 (ground), 289 (flight), and 127 (parachute) samples, respectively, recorded with a sampling rate of 1 Hz. The frequency comb is intentionally unlocked 40 s before lift-off to avoid uncontrolled behavior of the feedback loops during vibrations caused by the launch. Middle: Altitude profile of the sounding rocket flight. Bottom: Acceleration during lift-off and reentry of the sounding rocket. The iodine reference and the frequency comb are locked on ground, during μg , and on the parachute.

FOKUS II. At lift-off, the sounding rocket was accelerated by the first motor stage with a peak thrust of 82.4 ms^{-2} ($8.4g$) for 12 s and a second motor stage with a peak thrust of 118 ms^{-2} ($12g$) for another 44 s. After 65 s the μg phase of the sounding rocket flight started in a parabolic flight with an apogee of 239.6 km reached at 251 s after lift-off. The μg phase ended with the reentry of the sounding rocket about 467 s after lift-off with a peak deceleration of 120 ms^{-2} ($12.2g$), followed by a parachute phase starting at 585 s. At 810 s, the payload landed with an impact deceleration of 206 ms^{-2} ($21g$).

During countdown, JOKARUS was locked to the transition R(56)32-0: a_1 for about 100 s before lift-off (Fig. 7). During the vibration in the ascent of the rocket, the frequency lock could not be maintained. At 61 s after lift-off, a μg -timer signal was received that triggered the autolock that searched and found the transition R(56)32-0 (see

Fig. 3) and restabilized the iodine reference to the component a_1 20 s after the μg -timer signal was received. The beat note with the frequency comb was recorded for 4 min and 13 s until reentry, when the lock was lost again due to vibrations during the impact of the payload into the atmosphere. After reentry, the autolock algorithm relocked the iodine reference again and the laser frequency remained locked to the transition $R(56)32-0:a_1$ for 2 min and 5 s during parachute descent until impact on the ground. Notably, we could operate JOKARUS as well as FOKUS II right after the recovery of the payload on the day of the flight.

The mean values of the beat-note time records between JOKARUS and the frequency comb taken on the ground, during flight, and on the parachute, shown in Fig. 7, are 30.982 (4), 30.996 (3), and 31.002 (4) MHz, where the numbers in parentheses are the numerical value of the Allan deviation $\sigma(\tau = 1 \text{ s})$ referred to the corresponding last digits of the quoted mean frequency. We choose to state the Allan deviation instead of the standard error of the mean because of the Flicker noise in the data that is dominated by the instability of the LNCSAC over the measured time intervals; cf. Fig. 6.

In the following, we calculate the optical absolute frequency of the JOKARUS frequency reference, locked to transition $R(56)32-0:a_1$, from the beat-note data recorded during the mission and the parameters of the frequency comb, and compare the result to the absolute frequency of the transition $R(56)32-0:a_{10}$ reported in the literature. The absolute frequency of JOKARUS at 532 nm follows from

$$f_{\text{JOKARUS}}(a_1) = 2(f_{\text{ceo}} + n f_{\text{rep}} + f_{\text{beat}} + f_{\text{AOM}}), \quad (1)$$

with the repetition rate f_{rep} and offset frequency f_{ceo} of the frequency comb of 100 and 20 MHz, respectively, and the mode number $n = 2\,816\,297$. A frequency of $f_{\text{AOM}} = 75 \text{ MHz}$ is added to account for a frequency shift caused by the frequency offset between the pump and the probe beam.

To compare the result with the absolute frequency of the component a_{10} that is predominantly reported in the literature, we subtract the frequency offset of $\Delta f_{a_{10}-a_1} = 571.5420 (15) \text{ MHz}$ between lines a_1 and a_{10} given in [34] and give the difference to the absolute frequency $f[a_{10}, R(56)32 - 0] = 563\,260\,223\,513 (5) \text{ kHz}$ adopted by the CIPM [34]. The resulting frequency difference at 532 nm on the ground, during flight, on the parachute, and after recovery are

$$\begin{aligned} \Delta f_{\text{ground}} &= 6.8 (7.8)_{\text{stat.}} \text{ kHz}, \\ \Delta f_{\text{flight}} &= -20.7 (6.9)_{\text{stat.}} \text{ kHz}, \\ \Delta f_{\text{parachute}} &= -32.2 (8.7)_{\text{stat.}} \text{ kHz}, \\ \Delta f_{\text{recovery}} &= -23.8 (6.6)_{\text{stat.}} \text{ kHz}, \end{aligned}$$

where the numbers in parentheses are the numerical value of the statistical uncertainty [35] referred to the corresponding last digits of the quoted result.

The differences in the frequency offset between the different phases of the mission are larger than the frequency fluctuations observed on comparable periods of time during the characterization of the two instruments. The offsets arise from the uncertainties of the iodine reference and the CSAC. The contribution from the CSAC according to its specifications are 28-kHz ($\pm 5 \times 10^{-11}$) frequency accuracy and 30-kHz magnetic sensitivity ($9 \times 10^{-11}/\text{G}$ with variation of up to 0.6 G during the flight). The contribution from the iodine reference might be caused by electronic offsets in the analog MTS error signal that might have shifted the lock point of the frequency control loop.

IV. CONCLUSIONS

In conclusion, we build an autonomous absolute optical frequency reference based on rovibronic transitions in molecular iodine and operate this frequency reference on a sounding rocket flight, where its autonomous operation can be verified by a beat-note measurement with an optical frequency comb.

With this mission, key components for future application of optical clocks envisioned for space applications are demonstrated in a short, ballistic space flight.

The performance of the iodine reference does not reach the expected performance due to excessive PM/AM conversion of laser frequency noise to amplitude noise. This limitation in the signal-to-noise ratio can be overcome by an adapted balanced detection scheme or laser sources with reduced frequency noise, such as the Nd:YAG NPRO laser or diode lasers with optical feedback from an external cavity [36]. The long-term instability of the iodine reference will be investigated and the system's performance may be improved by intensity stabilization and cancellation of residual amplitude modulation. Potential for further development lies in the miniaturization of the system and the reduction of mass, size, and power consumption. With these improvements, an iodine reference is a viable option for future space missions that rely on frequency-stabilized laser systems and benefit from an absolute frequency reference.

ACKNOWLEDGMENTS

This work is supported by the DLR Space Administration with funds provided by the Federal Ministry for Economic Affairs and Energy (BMWi) under Grant No. DLR 50 WM 1646. The authors thank Josef Lazar and Jan Hrabina from ISI Brno for contribution of the unsaturated iodine absorption cell and Matthias Schoch from Humboldt-University Berlin for the design, assembly, and integration of electronics. The iodine spectroscopy was integrated in the Laboratory of Enabling Technologies

at Airbus Defence and Space in Friedrichshafen, where support by Dennis Weise and Alexander Sell is highly appreciated. We also thank Airbus DS for technical support throughout the mission, as well as SSC, MORABA, and OHB for assistance during the launch campaign.

-
- [1] B. S. Sheard, G. Heinzel, K. Danzmann, D. A. Shaddock, W. M. Klipstein, and W. M. Folkner, Intersatellite laser ranging instrument for the GRACE follow-on mission, *J. Geod.* **86**, 1083 (2012).
- [2] F. Flechtner, K.-H. Neumayer, C. Dahle, H. Dobsław, E. Fagiolini, J.-C. Raimondo, and A. Güntner, What can be expected from the GRACE-FO laser ranging interferometer for earth science applications? *Surv. Geophys.* **37**, 453 (2016).
- [3] P. Amaro-Seoane *et al.*, Laser interferometer space antenna, *Laser Phys.* **15**, 1056 (2017).
- [4] P. Kómár, E. M. Kessler, M. Bishof, L. Jiang, A. S. Sørensen, J. Ye, and M. D. Lukin, A quantum network of clocks, *Nat. Phys.* **10**, 582 (2014).
- [5] G. Giorgi, T. D. Schmidt, R. Mata-Calvo, C. Fuchs, M. M. Hoque, J. Berdermaan, J. Furthner, C. Gunther, T. Schuldt, J. Sanjuan, M. Gohlke, M. Oswald, C. Braxmaier, K. Balidakis, G. Dick, F. Flechtner, M. Ge, S. Glaser, R. König, G. Michalak, M. Murboeck, M. Semmling, and H. Schuh, Advanced Technologies for Satellite Navigation and Geodesy, submitted to *Advances in Space Research* (2019).
- [6] R. Thompson, W. M. Folkner, G. de Vine, W. M. Klipstein, K. McKenzie, R. Spero, N. Yu, M. Stephens, J. Leitch, R. Pierce, T. T.-Y. Lam, and D. A. Shaddock, in *2011 Joint Conference of the IEEE International Frequency Control and the European Frequency and Time Forum (FCS) Proceedings* (IEEE, San Francisco, USA, 2011), Vol. 8, p. 1.
- [7] Q.-F. Chen, A. Nevsky, M. Cardace, S. Schiller, T. Legero, S. Häfner, A. Uhde, and U. Sterr, A compact, robust, and transportable ultra-stable laser with a fractional frequency instability of 1×10^{-15} , *Rev. Sci. Instrum.* **85**, 113107 (2014).
- [8] O. Gerberding, K.-S. Isleif, M. Mehmet, K. Danzmann, and G. Heinzel, Laser-frequency stabilization via a quasimonolithic Mach-Zehnder interferometer with arms of unequal length and balanced dc readout, *Phys. Rev. Appl.* **7**, 024027 (2017).
- [9] T. G. McRae, S. Ngo, D. A. Shaddock, M. T. L. Hsu, and M. B. Gray, Frequency stabilization for space-based missions using optical fiber interferometry, *Opt. Lett.* **38**, 278 (2013).
- [10] J. J. McFerran and A. N. Luiten, Fractional frequency instability in the 10^{-14} range with a thermal beam optical frequency reference, *J. Opt. Soc. Am. B* **27**, 277 (2010).
- [11] J. Olson, R. Fox, R. Brown, T. Fortier, T. Sheerin, C. W. Oates, and A. D. Ludlow, in *2017 Joint Conference of the European Frequency and Time Forum and IEEE International Frequency Control Symposium (EFTF/IFCS)* (IEEE, Besançon, France, 2017), Vol. 30, p. 32.
- [12] H. Shang, X. Zhang, S. Zhang, D. Pan, H. Chen, and J. Chen, Miniaturized calcium beam optical frequency standard using fully-sealed vacuum tube with 10^{-15} instability, *Opt. Express* **25**, 30459 (2017).
- [13] S. Zhang, X. Zhang, J. Cui, Z. Jiang, H. Shang, C. Zhu, P. Chang, L. Zhang, J. Tu, and J. Chen, Compact Rb optical frequency standard with 10^{-15} stability, *Rev. Sci. Instrum.* **88**, 103106 (2017).
- [14] G. Phelps, N. Lemke, C. Erickson, J. Burke, and K. Martin, Compact optical clock with 5×10^{-13} instability at 1 s, *Navigation* **65**, 49 (2018).
- [15] K. W. Martin, G. Phelps, N. D. Lemke, M. S. Bigelow, B. Stuhl, M. Wojcik, M. Holt, I. Coddington, M. W. Bishop, and J. H. Burke, Compact Optical Atomic Clock based on a Two-Photon Transition in Rubidium, *Phys. Rev. Appl.* **9**, 014019 (2018).
- [16] M. L. Eickhoff and J. L. Hall, Optical frequency standard at 532 nm, *IEEE Trans. Instrum. Meas.* **44**, 155 (1995).
- [17] A. Arie and R. L. Byer, Laser heterodyne spectroscopy of $^{127}\text{I}_2$ hyperfine structure near 532 nm, *J. Opt. Soc. Am. B* **10**, 1990 (1993).
- [18] A. Nevsky, R. Holzwarth, J. Reichert, T. Udem, T. Hänsch, J. Zanthier, H. Walther, H. Schnatz, F. Riehle, P. Pokasov, M. Skvortsov, and S. Bagayev, Frequency comparison and absolute frequency measurement of I_2 -stabilized lasers at 532 nm, *Opt. Commun.* **192**, 263 (2001).
- [19] J. Ye, L. S. Ma, and J. L. Hall, Molecular Iodine Clock, *Phys. Rev. Lett.* **87**, 270801 (2001).
- [20] Er Jun Zang, Jian Ping Cao, Ye Li, Cheng Yang Li, Yong Kai Deng, Chun Qing Gao, E. Zang, J. Cao, Y. Li, and C. Li, Realization of four-pass I_2 absorption cell in 532-nm optical frequency standard, *IEEE Trans. Instrum. Meas.* **56**, 673 (2007).
- [21] T. Schuldt, K. Döringshoff, E. V. Kovalchuk, A. Keetman, J. Pahl, A. Peters, and C. Braxmaier, Development of a compact optical absolute frequency reference for space with 10^{-15} instability, *Appl. Opt.* **56**, 1101 (2017).
- [22] K. Döringshoff, T. Schuldt, E. V. Kovalchuk, J. Stühler, C. Braxmaier, and A. Peters, A flight-like absolute optical frequency reference based on iodine for laser systems at 1064 nm, *Appl. Phys. B* **123**, 183 (2017).
- [23] A. Wicht, A. Bawamia, M. Krüger, C. Kürbis, M. Schiemangk, R. Smol, A. Peters, and G. Tränkle, Narrow linewidth diode laser modules for quantum optical sensor applications in the field and in space, *Proc. SPIE* **10085**, 10085 (2017).
- [24] C. Kürbis, “Extended-cavity diode laser master-oscillator-power-amplifier for precision iodine spectroscopy in space” (unpublished).
- [25] V. Schkolnik, K. Döringshoff, F. B. Gutsch, M. Oswald, T. Schuldt, C. Braxmaier, M. Lezius, R. Holzwarth, C. Kürbis, A. Bawamia, M. Krutzik, and A. Peters, JOKARUS – design of a compact optical iodine frequency reference for a sounding rocket mission, *EPJ Quantum Technol.* **4**, 9 (2017).
- [26] G. Di Domenico, S. Schilt, and P. Thomann, Simple approach to the relation between laser frequency noise and laser line shape, *Appl. Opt.* **49**, 4801 (2010).
- [27] P. C. Hobbs, Ultrasensitive laser measurements without tears, *Appl. Opt.* **36**, 903 (1997).

- [28] F. B. Gutsch, <https://github.com/trimitri/jokarus>.
- [29] M. Lezius *et al.*, Space-borne frequency comb metrology, *Optica* **3**, 1381 (2016).
- [30] R. Holzwarth, A. Nevsky, M. Zimmermann, T. Udem, T. Hänsch, J. von Zanthier, H. Walther, J. Knight, W. Wadsworth, P. Russell, M. Skvortsov, and S. Bagayev, Absolute frequency measurement of iodine lines with a femtosecond optical synthesizer, *Appl. Phys. B* **73**, 269 (2001).
- [31] R. Walser and P. Zoller, Laser-noise-induced polarization fluctuations as a spectroscopic tool, *Phys. Rev. A* **49**, 5067 (1994).
- [32] D. H. McIntyre, J. Cooper, R. Walser, and C. E. Fairchild, Diode-laser noise spectroscopy of rubidium, *Opt. Lett.* **18**, 1816 (1993).
- [33] T. Hori, A. Araya, S. Moriwaki, and N. Mio, Formulation of frequency stability limited by laser intrinsic noise in feedback systems, *Appl. Opt.* **48**, 429 (2009).
- [34] CIPM, Recommended values of standard frequencies for applications including the practical realization of the metre and secondary representations of the definition of the second, https://www.bipm.org/utls/common/pdf/mep/M-e-P_12_532.pdf.
- [35] The given uncertainty is calculated from the Allan deviation of the corresponding beat-note time-record and the uncertainty of $\Delta f_{a_{10}-a_1}$ stated in the text, i.e. as $u(\Delta f) = \sqrt{2^2 \sigma^2(\tau = 1 \text{ s}) + u^2(\Delta f_{a_{10}-a_1})}$ where a factor of 2 accounts for the frequency doubling.
- [36] W. Lewoczko-Adamczyk, C. Pyrlik, J. Häger, C. Schwertfeger, A. Wicht, A. Peters, G. Erbert, and G. Tränkle, Ultranarrow linewidth DFB-laser with optical feedback from a monolithic confocal Fabry-Perot cavity, *Opt. Express* **23**, 9705 (2015).